

## Article

# Experimental and Numerical Calculation Study on the Slope Stability of the Yellow River Floodplain from Wantan Town to Liuyuankou

Hao Wang <sup>1</sup>, Qing Hu <sup>1</sup>, Weiwei Liu <sup>2</sup>, Liqun Ma <sup>3,\*</sup>, Zhiying Lv <sup>1</sup>, Hongyu Qin <sup>4</sup> and Jianbo Guo <sup>1</sup><sup>1</sup> School of Civil and Architectural Engineering, Henan University, Kaifeng 475004, China<sup>2</sup> Engineering Technology Research Center for Embankment Safety and Disease Control, Ministry of Water Resources, Zhengzhou 450003, China<sup>3</sup> The College of Geography and Environmental Science, Henan University, Kaifeng 475004, China<sup>4</sup> College of Science and Engineering, Flinders University, Adelaide 5042, Australia

\* Correspondence: malq@henu.edu.cn; Tel.: +86-1783-9271-038

**Abstract:** More than two million people live on the floodplains along the middle and lower streams of the Yellow River. The rapid development of industry and agriculture on both sides of the Yellow River has caused serious pollution of the floodplain soil. Erosion by water has led to the destruction of the floodplain which has not only compressed people's living space but also resulted in a large amount of sediment containing heavy metals entering the river, aggravating water pollution. To further study the law governing the release of pollutants in soil, this work, based on field surveys of the Yellow River floodplain slopes from Wantan town to Liuyuankou, was focused on determining the failure mechanism and laws for the floodplain slope through the combination of a flume experiment and numerical calculations. The results showed that the floodplain slopes, composed of clay and silty sand, presented an interactive structure. Under the action of water erosion, the slope was first scoured to form a curved, suspended layer structure, and then the upper suspended layer toppled. The bank stability coefficient decreased by about 65% when the scour width increased from 0.07 m to 0.42 m, and the water content increased from 20% to 40%. For the failure characteristics, the angle of the failure surface was negatively correlated with the scour width, and the distance from the top failure surface to the bank edge was about 2.5 times that of the scour width.

**Keywords:** floodplain; slope; scour; flume experiment; numerical calculation



**Citation:** Wang, H.; Hu, Q.; Liu, W.; Ma, L.; Lv, Z.; Qin, H.; Guo, J. Experimental and Numerical Calculation Study on the Slope Stability of the Yellow River Floodplain from Wantan Town to Liuyuankou. *Toxics* **2023**, *11*, 79. <https://doi.org/10.3390/toxics11010079>

Academic Editors: Qiting Zuo, Wei Zhang, Jing Liu and Lin Gong

Received: 3 December 2022

Revised: 6 January 2023

Accepted: 10 January 2023

Published: 14 January 2023



**Copyright:** © 2023 by the authors. Licensee MDPI, Basel, Switzerland. This article is an open access article distributed under the terms and conditions of the Creative Commons Attribution (CC BY) license (<https://creativecommons.org/licenses/by/4.0/>).

## 1. Introduction

Pollution caused by heavy metals in soil is attracting more and more attention. The rapid development of industry and agriculture along the lower Yellow River has increased the number of heavy metals in the soil [1,2]. When the heavy metal content in bank soil accumulates to a certain extent, it causes damage to riparian organisms, and the numbers of plant species significantly decrease with increases in the heavy metal concentration [3–5]. In recent years, the collapse of the bank has resulted in polluted soil continuously entering the Yellow River, causing serious pollution in the water body. In addition, some studies have found that the riverbank can intercept the polluted sediments carried by the upstream river, but when the riverbank is damaged, these pollutants re-enter the river [6,7]. Zhao surveyed ten major tributaries along the middle and lower reaches of the Yellow River and found that all of the lower tributaries had poor water quality and that the pollutants mainly came from industry and agriculture [8]. Walling found that 90 percent of heavy metals in the water were associated with suspended solids and sediments [9]. Many scholars have studied the pollution of the Yellow River [10,11]. However, there is little research on the release law for soil pollutants resulting from erosion. This work was undertaken to lay a

foundation for further research on the release of pollutants by studying the failure law and failure rate for the slope of the Yellow River floodplain.

The Yellow River is about 5464 km long and is one of the longest rivers in the world [12]. Xiaolangdi Dam is the last cascade reservoir in the main stream of the Yellow River and is located at the exit from the last gorge in the middle stream of the Yellow River. The important roles of the dam are to store water and hold back sand. Compared to the average from 1956 to 2016, the measured annual sediment transport volume at Xiaolangdi decreased by 90.5% in 2021 [13]. As the sediment entering the downstream channel has been greatly reduced, the sand-carrying capacity of the current cannot be satisfied, and the downstream riverbank is being scoured [14–17]. The continuous collapse of the slope is causing a number of environmental problems and increasing the risk of damage to infrastructure along the riverbank [18–20]. It is expected that the lower reaches of the Yellow River will continue to be strongly scoured, with the concave bank being the most strongly effected, followed by the straight bank.

Research on failure mechanisms has developed from homogeneous to multi-layer slopes. Das and others studied the scour damage in cohesive homogeneous slopes [21–23]. Yu conducted scouring experiments on non-cohesive and cohesive homogeneous banks, revealing the iterative cycle of bank erosion and riverbed deformation [24]. Hazari et al. analyzed the stability of two different cohesive soil slopes [25–27]. Dapporto studied the failure mechanism in a riverbank with a dual structure of sand and clay [28]. Yodsomjai studied the stability of double-layer conical slopes [29]. Li evaluated the stability of a three-layer slope composed of two cohesive soil layers and backfill soil [30]. However, previous studies on stratified slopes rarely go beyond three layers, while the floodplain slopes of the lower Yellow River show an interactive structure because the numerous floods have resulted in the silty sand and clay carried by the river being alternately deposited on the river beach. Although the Yellow River floodplain is rapidly collapsing, the failure pattern and characteristics of the floodplain slope composed of silty sand and clay interlayers have not been extensively studied. The slope of the Yellow River floodplain presents a typical interactive stratified structure, and slopes with special structures have not been widely studied. Gusman suggested that one of the important factors in slope stability analysis is water content [31]. Hooke and Casagli et al. stated that soil moisture content is essential to beach erosion [32–34]. Gu highlighted the influence of different irrigation methods on landslides [35]. In light of this work, it is necessary to consider the influence of water content in the research process.

There has been much research undertaken on river scour [36,37]. Pandey studied the erosion of piers by water flow [38]. Huang established a model for sediment transport caused by flooding [39]. Yang studied the operational impact of the Three Gorges Dam on river scour [40]. Yan et al. studied the protective effect of vegetation on gully banks through scouring experiments [41]. Another study discussed the sediment transport trajectory [42]. Dey conducted a scouring experiment with a bend flume and found that cross flow is an important factor in bank erosion [43]. Limit analysis theory with strict upper- and lower-limit solutions is often used in slope stability research [44,45]. Rao proposed a three-dimensional slope stability analysis method based on limit analysis [46]. Maghous analyzed the stability of rock slopes [47]. Huang used the upper limit theorem from limit analysis to draw a hazard map of shallow landslides [48]. Vasquez used a two-dimensional model to simulate scour and deposition along curved channels [49]. Karssenbergh studied sediment transport in flood plains using a three-dimensional numerical model [50]. It can be seen from the previous studies that the research methods used are mainly numerical simulation and experimental methods. In this paper, soil collected from a field investigation was used to conduct a reduced model erosion test to study the failure mechanism for the floodplain slope. However, the physical model test is easily limited by size, resulting in different results [51,52]. Although parameters can be set according to different situations in the numerical simulation, the actual working conditions are complex [53,54]. In this paper, to take full advantage of both methods, the flume experiment and numerical calculation

are combined to study the failure mechanism and pattern of floodplain slope. To make the conditions of the experiment closer to those of the slope in its natural state, soil collected from field investigation is used.

## 2. Materials and Methods

### 2.1. Study Area

The study area is located between Zhengzhou and Kaifeng ( $113^{\circ}58' \sim 114^{\circ}23' \text{ E}$ ,  $34^{\circ}50' \sim 35^{\circ} \text{ N}$ ), the core development cities of the Central Plains, and is an important agricultural planting area (Figure 1) [55,56]. Due to the flat terrain, sediment carried by the Yellow River from the upper reaches is constantly deposited in the area, forming the famous overhanging river. The climate in this region is a temperate monsoon climate, characterized by cold and dry winters and high temperatures and rain in summer. The average annual precipitation and temperature are 636 mm and  $15^{\circ} \text{ C}$ , respectively, and this area is rich in biological resources, with nearly 800 and 60 kinds of plants and animals, respectively. The economic development of the region is dominated by traditional industries, such as the chemical and energy industries, and crop cultivation, which have a significant impact on the ecological environment of the lower Yellow River [57]. Cultivated land is widely distributed in this area, and the soil is mainly loam, clay, and silt. However, due to the influence of climate and precipitation, wheat and corn are the main crop in winter and summer, respectively. Meanwhile, the sediment from the Loess Plateau is deposited to form floodplains which also have become significant land resources for agriculture. However, due to the operation of the Xiaolangdi Dam, the floodplain keeps retreating. Wang analyzed satellite images of the Yellow River from Huayuankou to Liuyuankou and found that nearly  $32.08 \text{ km}^2$  of farmlands on the floodplain were destroyed over 13 years [58].

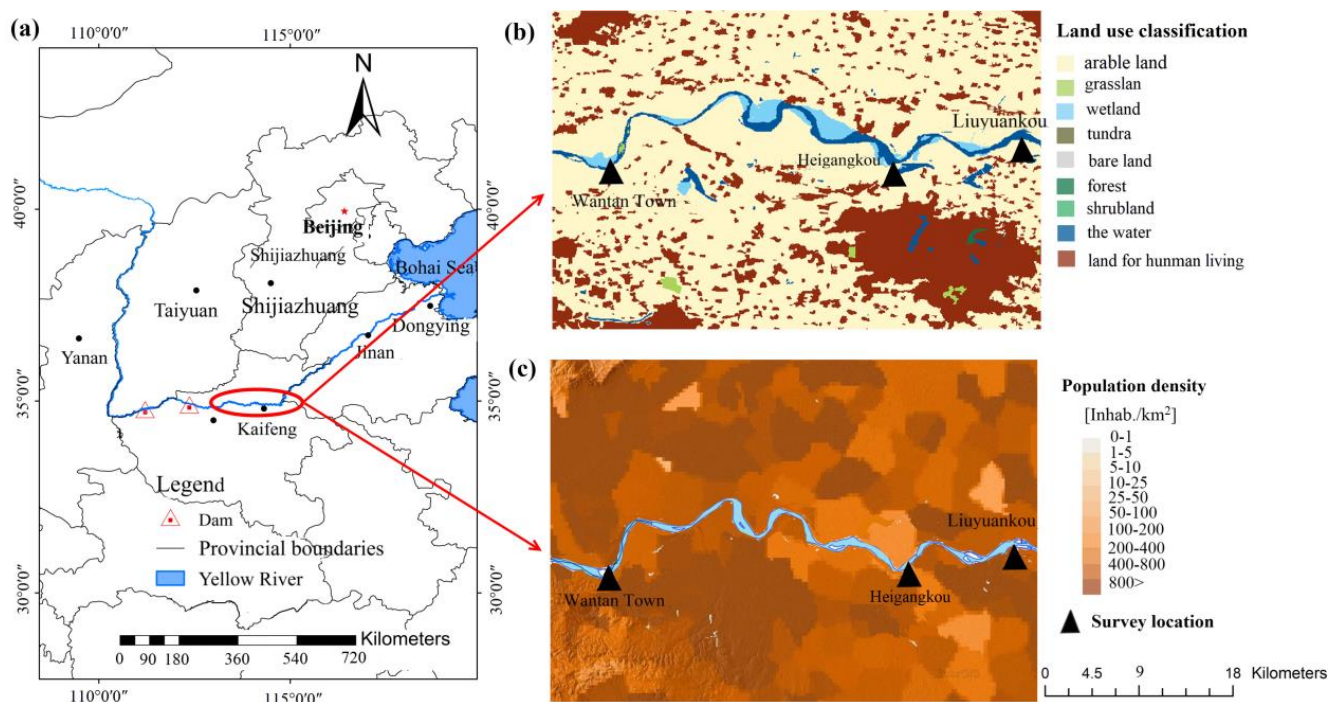


**Figure 1.** The location of the study area: (a) specific locations of the study area; (b) land use classification of the study area; (c) population density of study area.

### 2.2. Field Investigation

Thorne and Xia found that the shear strength reflects the slope stability [59,60]. To better understand the floodplain soil structure and mechanical properties, a field investigation, including soil sampling and scanning with SIR4000 geological radar, was carried

out on the floodplain slopes from Wantan Town to Liuyuankou. Simultaneously, according to the erosion situation in the area, an investigation point was selected in Wantan Town, Heigangkou, and Liuyuankou, respectively (Figure 1). As shown in Figure A1, the geological radar was used to scan the floodplain slope parallel to the failure surface, and a total of 18 cross-sections from Wantan Town, Heigangkou, and Liuyuankou were swept. Given the actual situation of the floodplain, the sampling points were selected in the places where the collapse is prominent, and six cross-sections were selected for sampling (Table A1). Layered sampling was used, as the floodplain slope presents an interactive structure. To correspond to the scan results of geological radar, the sampling position and altitude were recorded strictly for each sampling. Undisturbed soil was sampled with a ring knife and sealed with plastic film, then placed in a plastic box. Additionally, the scattered soil was placed in a well-sealed plastic bag.

### 2.3. Laboratory Tests and Soil Types

The laboratory test is a standard method for classifying soil and understanding the physical and mechanical properties of soil, and the test procedure followed the geotechnical test method standards strictly [61]. The contents measured mainly included moisture content, density, specific gravity, shear strength index, and plasticity index.

### 2.4. The Scouring Experiment

The collapse of the floodplain slope directly threatens the safety of the Yellow River levee. Additionally, Heigangkou is located in Kaifeng, where levees have repeatedly broken in the past. The S-shaped flume following the actual bank size of the Heigangkou section was used to simulate the erosion process of the convex, concave, and straight banks, to study the failure pattern and mechanism of the floodplain slope (Figure 2).

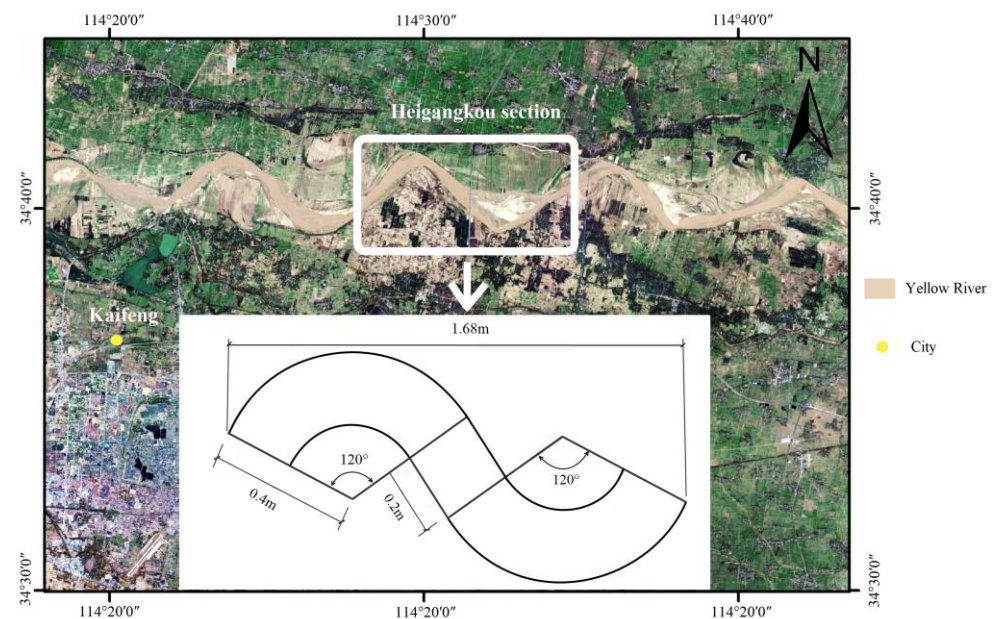


**Figure 2.** Schematic diagram of flume size.

Three profile positions were selected in this experiment, as shown in Figure 3a. A camera was set up on the convex, concave, and straight banks to capture the failure process. Earth pressure sensors were buried at the bottom of the concave and straight banks, and the measuring accuracy of the earth pressure box is 0–0.4 MPa. To prevent water from scouring the start and end of the slope, gravels were paved in the water inlet and outlet of the flume (Figure 3). The water outlet of the flume was provided with a water baffle which was used to control the water level height by changing its position at the same time (Figure 3a). The detailed description of the experiment equipment is shown in Table A2.

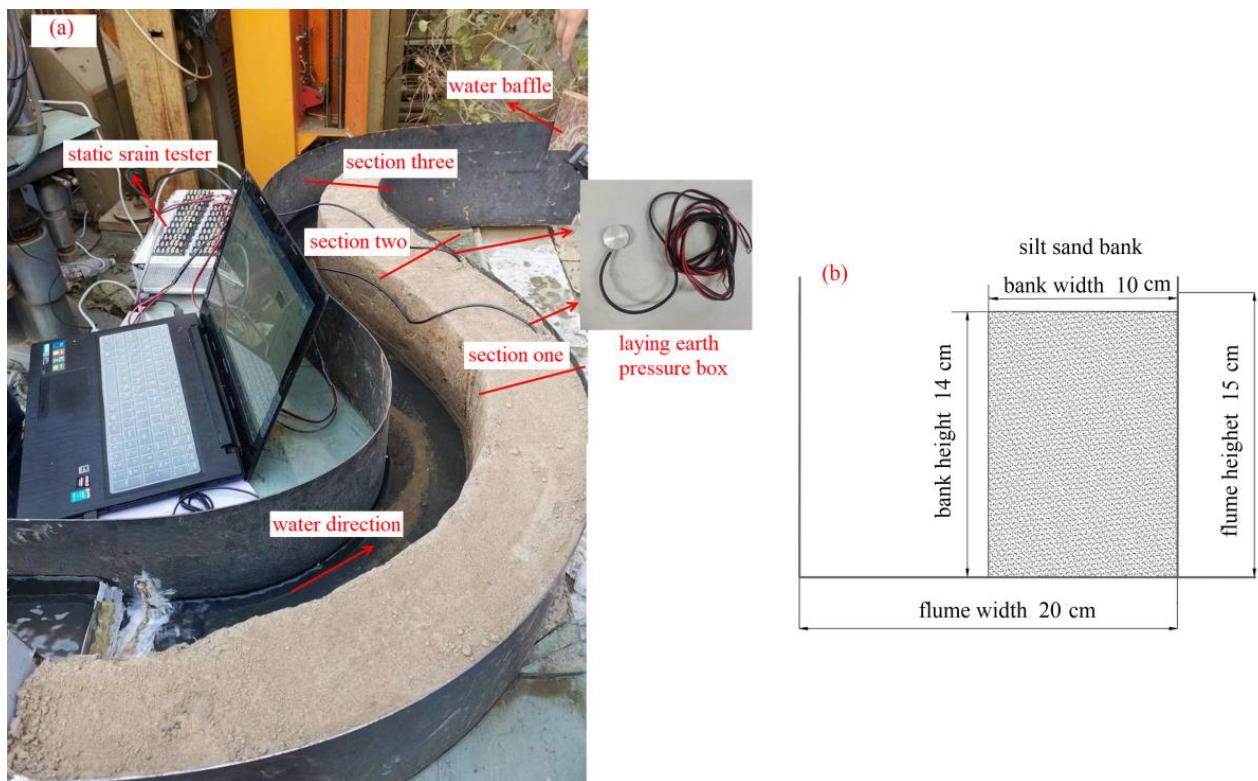


**Figure 3.** Actual diagram of the scouring experiment: (a) the layout of the scouring experiment; (b) side views of the flume.

The river gradient and incoming water flow were taken as variables, and three working conditions were designed as a control. Each working condition was scoured for 1 h (the specific experimental design is listed in Table 1). Simultaneously, to simulate scouring damage when the water level changes, the water level was set to two heights (5 and 10 cm) and changed every 10 min. Each working condition required 75 kg of soil, collected from Wantan Town to Liuyuankou, and the size of the final experiment bank structure is illustrated in Figure 3b. The floodplain slopes present an interactive layered structure in their natural state; however, it was difficult to lay the clay directly. Therefore, the silty sand and clay were mixed as the experiment soil. To achieve the actual working condition density, it was necessary to tamp when laying the mixed soil.

**Table 1.** The detailed arrangement of experimental groups.

Working Condition	Bank Height (cm)	Flow (L/s)	Bank Angle (°)	River Gradient	Scouring Time (h)
1	14	0.5	90	0.01	1
2	14	0.5	90	0.02	1
3	14	0.5	90	0.03	1
4	14	0.8	90	0.01	1
5	14	1.2	90	0.01	1

### 2.5. Numerical Simulation

The limit analysis method was used to validate the failure pattern of a straight bank. Additionally, the effects of the scour width on the stability of the interactive layered slope were also analyzed. OptumG2 is a geotechnical software that integrates limit and finite element analysis and can simulate complex problems with nonlinear failure criteria [62–65]. Tschuchnigg and Sloan introduced the principle, advantages, and disadvantages of software in detail [45,66]. Every simulation in this paper required five iterations, and when the iteration number raised, the unit number increased from 5000 to 10,000.

### 3. Results

#### 3.1. Field Investigation and Geotechnical Test Results

The bank presents a vertical stratified structure, and bank soil is roughly divided into brown and yellow soils (Figure 4). A scan result in Wantan Town is presented on the right side of Figure 4. Because different soils correspond to individual conductivity properties, nearly all the scan results of 18 sections showed a vertically layered structure.

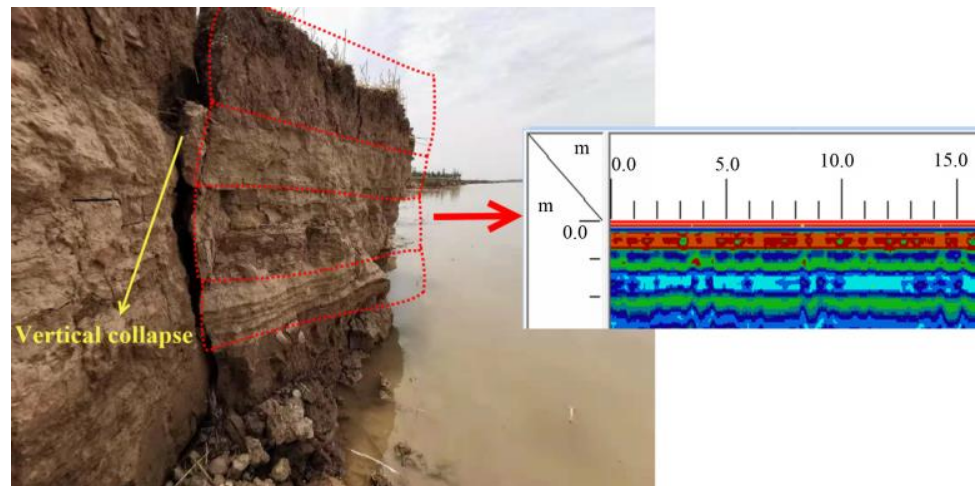


Figure 4. The scan result of a section in Wantan Town.

Owing to the plasticity indexes above 17 (shown in Table 2), the soil was classified as clay in combination with relevant classification standards [67]. The yellow soil was first subjected to a sieving test, and then the particle gradation of the soil with particle size below 0.075 mm was determined by the densitometer method. Finally, the drawn particle gradation curve is shown (Figure 5). The particle size greater than 0.075 mm and smaller than 0.005 mm did not exceed 50% and 10% of the total weight, respectively. The plasticity index obtained from the liquid–plastic limit test was less than 10, so this soil was classified as silty sand according to the standard [67].

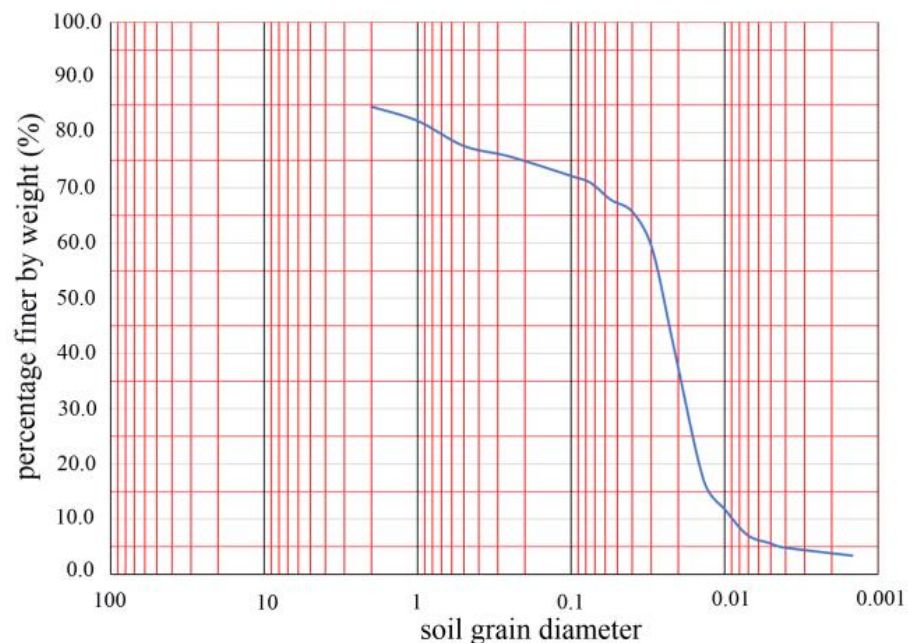


Figure 5. The particle gradation curve of the soil, whose scan color is blue.

**Table 2.** Part test results of the brown soil.

Soil Label	Sampling Location	Depth (cm)	Moisture Content (%)	Dry Density (g·cm <sup>-3</sup> )	Wet Density (g·cm <sup>-3</sup> )	Ip	Shear Strength	
							C (kPa)	φ (°)
1	Wantantown	25	21.15	1.66	2.009	18.2	36.5	28.6
2	Wantantown	86	35.61	1.40	1.851	23.6	26.36	18.56
3	Heigangkou	30	16.7	1.57	1.836	21.1	49.1	32.3
4	Heigangkou	55	25.55	1.71	2.113	19.4	31.3	26.5
5	Liuyuankou	93	28.81	1.63	2.232	21.7	39.1	23.63
6	Liuyuankou	137	39.71	1.49	1.910	18.8	36.51	25.1

Symbols: Ip = Plasticity index.

### 3.2. Scouring Experiment Result

#### 3.2.1. Failure Pattern

Figure 6a shows the bank failure schematic diagram of concave, straight, and convex banks under working condition 2. The erosion degree of the concave bank is greater than that of the straight bank and the convex bank, and the convex bank is silted. According to Figure 6b, it can be found that the slope toe was scoured to form an arc-shaped scouring surface, which was attributed to the presence of clay and the pseudo-cohesion of silty sand. To further understand erosion characteristics under the different variables and compare with previous studies, the scour height, L<sub>1</sub> and width, L<sub>2</sub>, accurate to millimeters, were introduced.

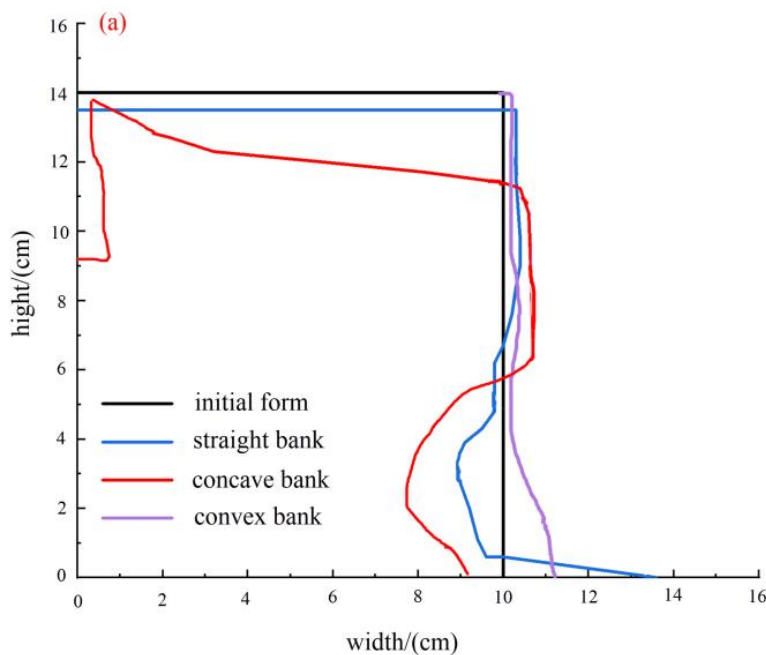


**Figure 6.** Bank failure pattern: (a) failure schematic diagram of slopes under working condition 2; (b) actual diagram of the concave bank under working condition 2 (L<sub>1</sub>: the scour height, L<sub>2</sub>: the scour width).

#### 3.2.2. Variation of Scour Width and Height

Figure 7a shows that when the channel gradient equaled 0.01, the concave and straight banks were all eroded because of the weak circulation intensity caused by the low water velocity. As the channel gradient increased from 0.01 to 0.03, the scour width of the concave bank gradually enhanced. On the contrary, the convex bank which kept depositing from the channel gradient equaled 0.03.

Figure 7b shows that with the increase in incoming water flow, there was no deposition in the straight and convex banks. Wang found that when the water flow increased to a certain extent, the straight and convex banks were eroded [68].

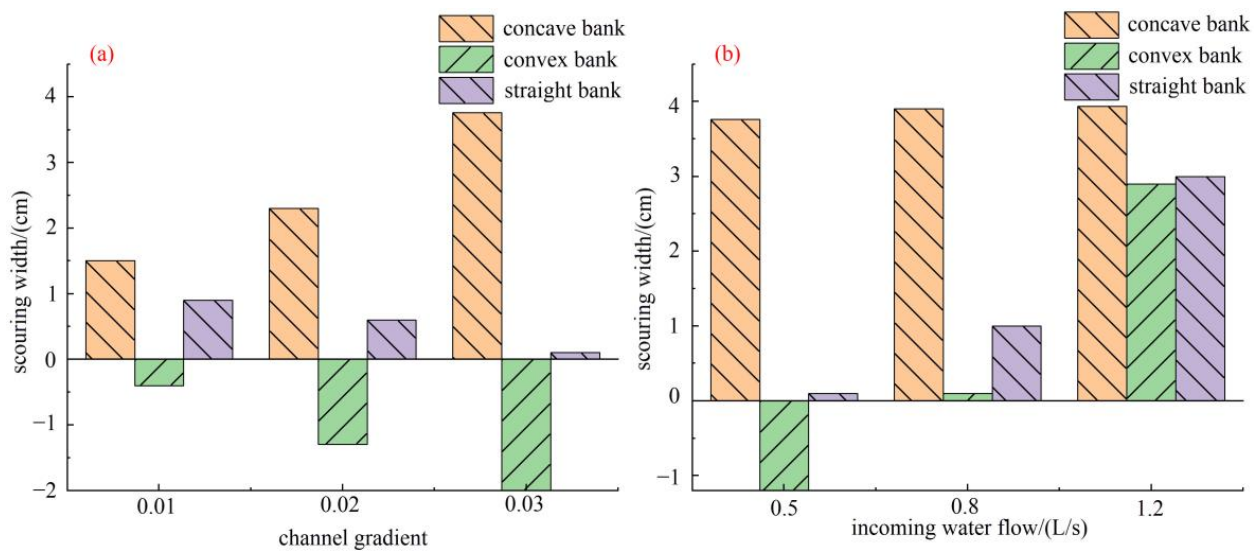


**Figure 7.** (a) The scour width varies when the channel ratio is a variable. (b) The scour width varies when incoming water flow is a variable.

### 3.2.3. Variation of Earth Pressure

The change of the internal earth pressure from the experiment’s start to the experiment’s end is shown in Figure 8. Two factors affect earth pressure in the experiment process; earth pressure increases with an increase in soil water content, but water erosion decreases earth pressure. The earth pressure increased first and then decreased (Figure 8). This appearance indicated that the water content in the early stage had a more significant impact than water flow erosion. In the later period, the earth pressure decreased when the water content changed very little. In combination with the video recorded for the experiment, the slope collapsed when the earth pressure was less than before the experiment.

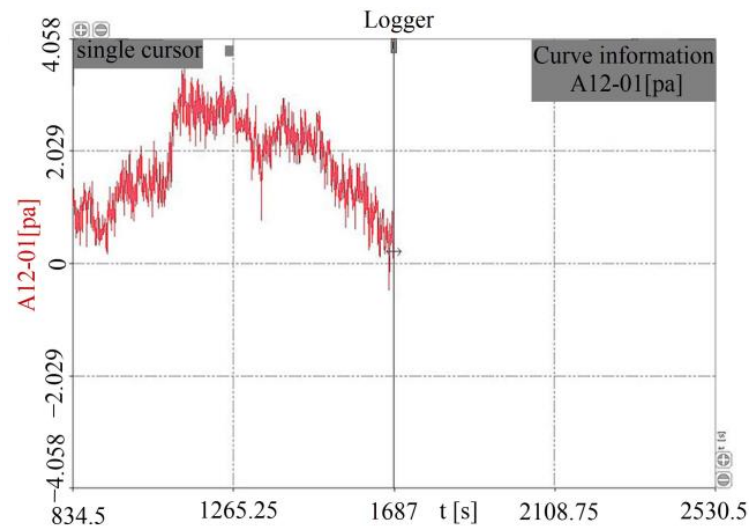


**Figure 8.** Earth pressure curve.

## 3.3. Numerical Results

### 3.3.1. Establishing the Slope Model

According to the flume experiment, the vertical slope formed an arc-shaped suspended layer under water flow scour. An equal proportional slope model, based on the size of the arc-shaped suspended layer, was established using OptumG2. A generalized model of slope collapse was established, wherein  $H$ ,  $H_1$ ,  $b$ , and  $\alpha$  represent bank height, water level, the length of the failure surface to the bank edge, and the failure surface angle, as seen in Figure 9.

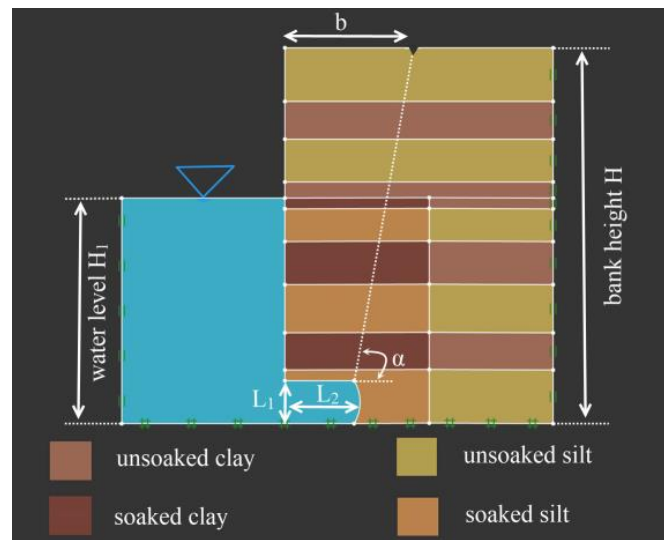


**Figure 9.** Generalized model of the bank collapse.

There was a significant difference in the soil moisture content between the soaked part and the higher part of the floodplain slope during the flume experiment and field survey. To consider the effect of water content on the bank stability, the water content was divided into 20 and 40%, corresponding to two kinds of soil strength, according to the data measured in the experiment. When simulating bank stability, the shear strength parameters for the experiment soils under the two water contents are shown in Table 3.

**Table 3.** Model parameters for simulating the failure mode.

H (m)	H <sub>1</sub> (m)	L <sub>1</sub> (m)	L <sub>2</sub> (m)	Moisture Content	Soil Type	C (kPa)	φ(°)	Dry Density (kN·m <sup>-3</sup> )	Wet Density (kN·m <sup>-3</sup> )
1.4	1	0.39	0.29	20%	clay	35	30	17	15
					silty sand	25	35	16	14
				40%	clay	15	10	18	15
					silty sand	10	20	17	14

### 3.3.2. Validation of the Bank Failure Pattern

The failure pattern of a straight bank after scouring (under test condition 5) was selected for validation using the OptumG2. The erosion height and width equal 0.39 and 0.29 m of the slope model in Figure 9, and the simulation results are stated in Figure 10.

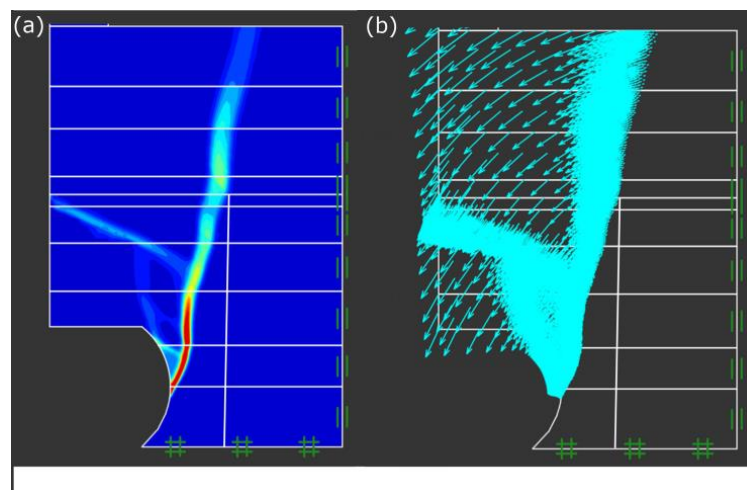


**Figure 10.** Validation result of the straight slope after scouring (under working condition 5): (a) the bank failure surface; and (b) displacement vector map.

The failure surface of the slope was almost vertical in Figure 10a. The simulated result was very similar to the failure mode of the scouring experiment; the upper suspended soil rotated and fell into the water under the action of gravity in Figure 10b.

### 3.3.3. Validation of the Influence of Scour Width on the Bank Stability

As the water flow continues to scour the slope, the scour width and height keep increasing, and the main reason for the bank collapse is severe local scour [69]. Therefore, it is critical to validate the influence of the scour width on slope stability. The bank model is shown in Figure 9, and the model parameters are shown in Table 4. The other variables remain unchanged when one variable changes. The simulation results are stated in Figures 11–13.

**Table 4.** Model parameters for simulating the effect of the scour degree on the stability coefficient.

H (m)	H <sub>1</sub> (m)	L <sub>1</sub> (m)	L <sub>2</sub> (m)	Moisture Content	Soil Type	C (kPa)	φ(°)	Dry Density (kN·m <sup>-3</sup> )	Wet Density (kN·m <sup>-3</sup> )
1.4	0.6 H	/	/	20%	clay	35	30	17	15
				20%	silty sand	25	35	16	14
				40%	clay	15	10	17	15
				40%	silty sand	10	20	17	14

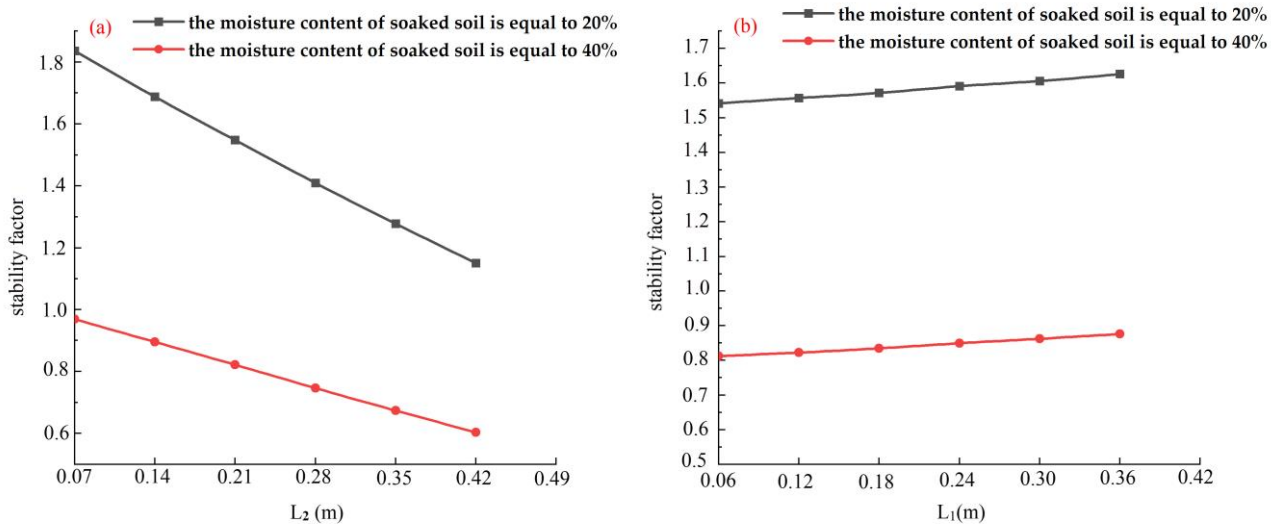


**Figure 11.** The effect of the scour degree on the bank stability: (a) the influence of the scour width on the stability coefficient; and (b) the effect of the scour height on the stability coefficient.

The stability coefficient of the bank decreases significantly with an increase in the scour width in Figure 11a. This was consistent with the scour experiment in that banks first collapsed with large scour width when the scour height was almost the same. Contrary to the scour width, the stability coefficient of the bank increased slightly with an increase in the scour height (Figure 11b). The bank soil strength significantly declines when the water content increases from 20% to 40% (Table 4). The bank stability coefficient decreases rapidly under the dual effects of an obvious decrease in the soil strength and an increase in scour width (Figure 11a).

When the scouring widths are 0.14, 0.21, 0.28 and 0.35m, respectively, the failure surface of the river bank is as shown in Figure 12. With an increase in the scouring width, the failure distance *b* of the shore top becomes larger, and the failure surface angle  $\alpha$  gradually decreases. The processing results of *b* and  $\alpha$  under six scour widths are shown in Figure 13. It is clear that  $\alpha$  is negatively correlated with *L*<sub>2</sub>, and *b* is about 2.5 times that of *L*<sub>2</sub>.

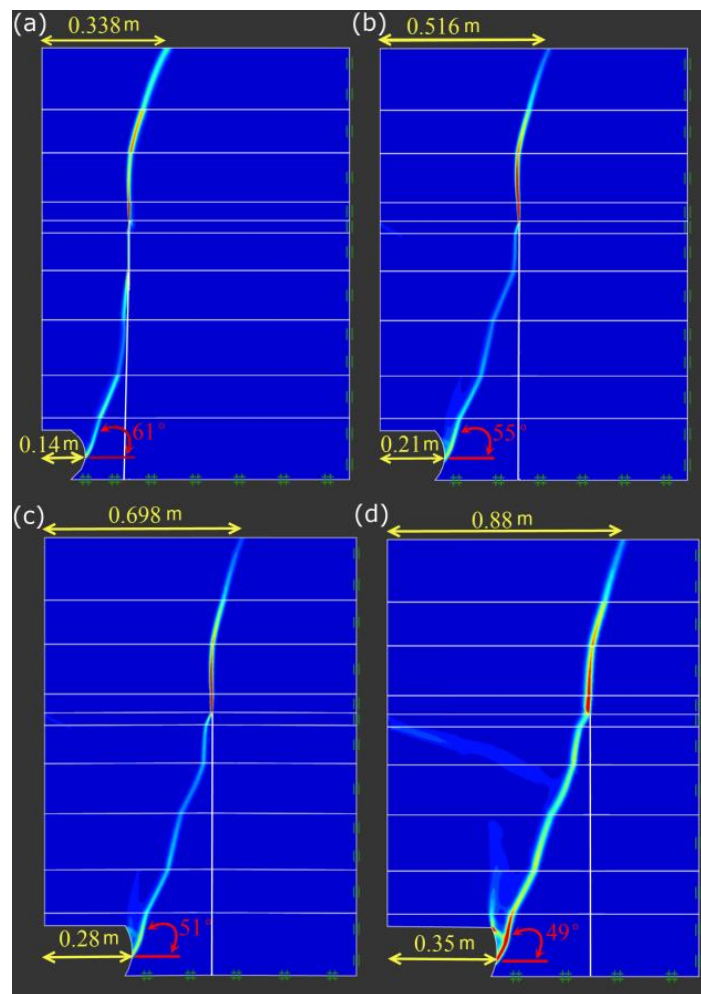


**Figure 12.** Variation of slope failure surface under four scour widths: (a) scour width is equal to 0.14 m, (b) scour width is equal to 0.21 m, (c) scour width is equal to 0.28 m, and (d) scour width is equal to 0.35 m (a).

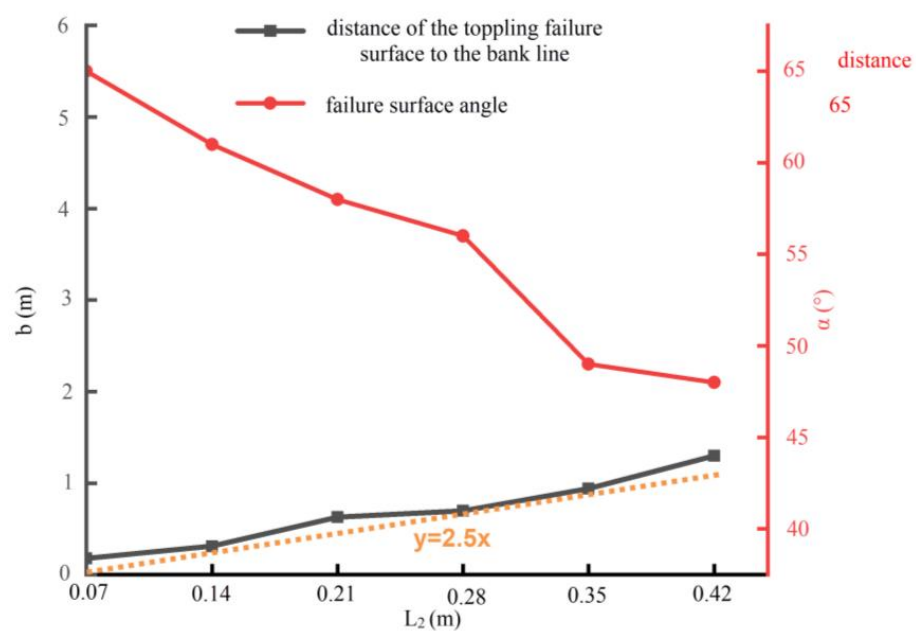


**Figure 13.** Variation in the angle of the failure surface and the length from the top failure surface to the bank edge with changes in scour width.

#### 4. Discussion

In the previous part of this paper, scour experiment and numerical simulations are combined to analyze the stability of interactive stratified slopes. In this part, the influence of water content and scour width on slope stability and bank failure law are discussed below.

In previous studies, water content was found to be an important factor affecting slope stability [27–31]. This article comes to the consistent conclusion from laboratory experiments that when the water content increased from 20% to 40%, the cohesion and internal friction angle of the clay decreased by about 60% and 67%, respectively, and the cohesion and internal friction angle of the silt soil decreased by about 61% and 43%, respectively (Table 4). Zhang studied the changes in water content and soil strength in the process of bank failure by using the numerical simulation method, and found that the water content increased rapidly in the initial stage; the change was relatively small in the later stage, and the soil strength of the bank decreased significantly [70]. The change in water content measured by Zhang is consistent with the results obtained by the earth pressure box in the scour experiment (Figure 8) which indicate that the variation trend in water content in multi-layer soil slope and single-layer soil slope is the same

According to the experimental observations, scouring is an important cause of bank failure. Numerical simulation results show that the bank stability coefficient decreased with the scour width increasing (Figure 11a). However, the stability coefficient of the bank increased slightly with an increase in the scour height. Zhang performed a systematic study on the failure of single-layer overhanging slopes and concluded that bank stability first decreases and then increases with an increase in erosion height [70]. This is because the stability of the sandy soil slope is poor, and the slope stability decreases rapidly after being soaked in water.

The slope was scoured to form an arc-shaped scouring surface under the action of water scour (Show in Figure 10), and the overhanging soil, broken through by the fissure, toppled when the bank slope was washed to a certain extent. Zhang summarized the failure pattern of single-layer bank slope and surmised that the length from the top failure surface to the bank edge is about twotimes of the scour width [70], which is smaller than the results of this paper (2.5 times). This difference may be caused by the clay layer in the stratified bank studied in this paper, which increases the integrity of the bank and makes the failure range of the top of the bank larger.

In this paper, failure law and the failure mechanism of floodplain slopes are studied through a flume experiment and numerical simulation. It is important to study the influence of scour width and water content on slope stability [27,28,70]. For now, only the general failure laws of the floodplain slope were obtained. The next step is to summarize the failure formulas which will also be calibrated with the bank failure data monitored in the field. Meanwhile, three-dimensional numerical simulation to study the erosion failure of the floodplain slope will be included in future research.

#### 5. Conclusions

Scouring of water flow leads to rapid degradation of the floodplain which compresses the production space of the people and seriously impacts the environment. In this paper, the failure mechanism and laws of floodplain slopes are studied by combining flume experiments and numerical simulation. A total of five conditions were designed in the flume experiment, and the failure characteristics of concave banks, convex banks, and straight banks in all conditions were recorded and analyzed. Meanwhile, through the establishment of an equal-scale bank model, the bank failure results of the numerical simulation and erosion experiment were compared. The main conclusions are as follows.

The main reasons for the floodplains' rapid collapse were that the slope toe was scoured, and the soil strength decreased rapidly; the bank stability coefficient decreased by about 65% when the scour width increased from 0.07 m to 0.42 m, and the water content increased from 20% to 40%.

The failure depth of the bank top is greatly affected by the scour width. It is found that the distance from the failure surface of the bank top to the edge,  $b$ , is about 2.5 times the scour width. Meanwhile, the failure surface angle diminishes with an increase in scour width.

Due to the rapid development of industry and agriculture on both sides of the river, the floodplain soil is seriously polluted, and floodplain slope collapse causes polluted soil to enter the river. The study of floodplain slope failure laws in this paper provides a new idea for the protection of the floodplain, and also lays a foundation for further study of the release law of pollutants in soil during floodplain slope failure.

**Author Contributions:** Conceptualization, H.W.; methodology, H.W., Q.H., Z.L. and L.M.; software, Q.H., Z.L. and H.Q.; validation, H.W., L.M., J.G. and W.L.; formal analysis, Q.H., H.Q. and L.M.; investigation, H.W., Q.H., Z.L. and J.G.; resources, L.M., W.L. and H.Q.; data curation, H.W. and Z.L.; writing—original draft preparation, Q.H. and Z.L.; writing—review and editing, H.W., Q.H. and L.M.; visualization, L.M. and W.L.; supervision, Z.L. and J.G.; project administration, H.W. and L.M.; funding acquisition, L.M. and Q.H. All authors have read and agreed to the published version of the manuscript.

**Funding:** This paper was supported by the General Program of China Postdoctoral Science Foundation (Grant No. 2020M672202), the Open Project Fund of the Embankment Safety and Disease Prevention Engineering Technology Research Center of the Ministry of Water Resources (Grant No. LSDP202202), and the Youth Program of Natural Science Foundation of Henan Province (Grant No. 212300410125).

**Institutional Review Board Statement:** Not applicable.

**Informed Consent Statement:** Not applicable.

**Data Availability Statement:** Data are available on request.

**Conflicts of Interest:** The authors declare that the research was conducted in the absence of any commercial or financial relationships that could be construed as a potential conflict of interest.

## Appendix A



**Figure A1.** Scanning the floodplain in Wantan Town using the geological radar.

**Table A1.** Soil sampling point locations.

Section Name	Latitude and Longitude	Sampling Depth (cm)
Wantantown Yangqiaovillage Heigangkou Nie zhuang Liu yunkou	113°56'41.08621" 34°52'52.67728"	25, 63, 86, 113
	113°52'4.84872" 34°51'54.74157"	13, 31, 58, 61, 123
	114°15'28.19616" 34°53'42.83452"	28, 58, 65, 131
	114°16'0.72747" 34°53'46.44162"	13, 39, 56, 113
	114°23'26.90973" 34°54'34.64414"	16, 68, 85, 140

**Table A2.** Introduction of experiment equipment.

Experimental Equipment	Style	Equipment Role	Range of Parameter Variation
S-shaped flume	welded with the 1.5 mm thick iron sheet	Simulating the erosion process of the different banks	—
Flow meter	Electromagnetic flowmeter	Controlling water flow	0.5–1.2 L/s
Static strain tester	DH3818Y	Processing of earth pressure data	−4.0–5.0 pa
Earth pressure boxes	Vibrating string earth pressure box	Measuring the change in earth pressure during the experiment	—
Cameras	Sony Alpha7C	Capturing the slope failure process	—
Water baffle	Granite plate	Controlling the water level height by changing its position	—
Graduated scale	Steel rule	Measuring the digital height	5–10 cm

## References

- Xiang, M.; Li, Y.; Yang, J.; Lei, K.; Li, Y.; Li, F.; Zheng, D.; Fang, X.; Cao, Y. Heavy metal contamination risk assessment and correlation analysis of heavy metal contents in soil and crops. *Environ. Pollut.* **2021**, *278*, 116911. [[CrossRef](#)] [[PubMed](#)]
- Li, Z.-H.; Li, Z.-P.; Tang, X.; Hou, W.-H.; Li, P. Distribution and Risk Assessment of Toxic Pollutants in Surface Water of the Lower Yellow River, China. *Water* **2021**, *13*, 1582. [[CrossRef](#)]
- Leuven, R.; Wijnhoven, S.; Kooistra, L.; Nooij, R.; Huibregts, M. Toxicological constraints for rehabilitation of riverine habitats: A case study for metal contamination of floodplain soils along the Rhine. *Large River* **2005**, *155*, 657–676. [[CrossRef](#)]
- Bai, J.; Xiao, R.; Cui, B.; Zhang, K.; Wang, Q.; Liu, X.; Gao, H.; Huang, L. Assessment of heavy metal pollution in wetland soils from the young and old reclaimed regions in the Pearl River Estuary. South China. *Environ. Pollut.* **2011**, *159*, 817–824. [[CrossRef](#)]
- Schipper, A.; Lotterman, K.; Leuven, R.; Ragas, A.; Kroon, H.; Hendriks, A. Plant communities in relation to flooding and soil contamination in a lowland Rhine River floodplain. *Environ. Pollut.* **2011**, *159*, 182–189. [[CrossRef](#)]
- Bai, J.; Jia, J.; Zhang, G.; Zhao, Q.; Lu, Q.; Cui, B.; Liu, X. Spatial and temporal dynamics of heavy metal pollution and source identification in sediment cores from the short-term flooding riparian wetlands in a Chinese delta. *Environ. Pollut.* **2016**, *219*, 379–388. [[CrossRef](#)]
- Le Gall, M.; Ayrault, S.; Evrard, O.; Laceby, J.; Gateuille, D.; Lefèvre, I.; Mouchel, J.M.; Meybeck, M. Investigating the metal contamination of sediment transported by the 2016 Seine River flood (Paris, France). *Environ. Pollut.* **2018**, *240*, 125–139. [[CrossRef](#)]
- Zhao, M.; Wang, S.; Chen, Y.; Wu, J.; Xue, L.; Fan, T. Pollution status of the Yellow River tributaries in middle and lower reaches. *Sci. Total Environ.* **2020**, *722*, 137861. [[CrossRef](#)]
- Walling, D.; Owens, P.; Carter, J.; Leeks, G.; Lewis, S.; Meharg, A.; Wright, J. Storage of sediment-associated nutrients and contaminants in river channel and floodplain systems. *Appl. Geochem.* **2003**, *18*, 195–220. [[CrossRef](#)]
- Zhang, P.; Qin, C.; Hong, X.; Kang, G.; Qin, M.; Yang, D.; Pang, B.; Li, Y.; Dick, R. Risk assessment and source analysis of soil heavy metal pollution from lower reaches of Yellow River irrigation in China. *Sci. Total Environ.* **2018**, *633*, 1136–1147. [[CrossRef](#)]
- Duan, H.; MA, J.; Peng, C.; Liu, D.; Wang, Y.; Li, X.; Ma, J. Characteristics and sources of soil heavy metal pollution in cultural parks of the lower Yellow River based on APCS-MLR and PMF models. *Environ. Sci.* **2022**, *43*, 2467–2475.
- Cui, J.; Zhu, M.; Liang, Y.; Qin, G.; Li, J.; Liu, Y. Land Use/Land Cover Change and Their Driving Factors in the Yellow River Basin of Shandong Province Based on Google Earth Engine from 2000 to 2020. *ISPRS Int. J. Geo-Inf.* **2022**, *11*, 163. [[CrossRef](#)]
- Yellow River Conservancy Commission of the Ministry of Water Resources. *Yellow River Water Resources Bulletin*; Yellow River Conservancy Commission of the Ministry of Water Resources: Zhengzhou, China, 2021; pp. 32–33.
- He, G.S.; Yao, S.M.; Jin, Z.W. Research on the atypical scour of the beach on the curved convex bank of the Jingjiang reach of the Yangtze River. *People's Yangtze River* **2011**, *42*, 4. (In Chinese)

15. Wang, Y.; Xia, J.; Deng, S.; Zhou, M.; Wang, Z.; Xu, X. Numerical simulation of bank erosion and accretion in a braided reach of the Lower Yellow river. *Catena* **2022**, *217*, 106456. [[CrossRef](#)]
16. Cheng, Y.; Xia, J.; Zhou, M.; Deng, S.; Li, D.; Li, Z.; Wan, Z. Recent variation in channel erosion efficiency of the Lower Yellow river with different channel patterns. *J. Hydrol.* **2022**, *610*, 127962. [[CrossRef](#)]
17. Chu, Z. The dramatic changes and anthropogenic causes of erosion and deposition in the lower Yellow (Huanghe) River since 1952. *Geomorphology* **2014**, *216*, 171–179. [[CrossRef](#)]
18. Yang, H.; Shi, C.; Cao, J. A Field Investigation on Gully Erosion and Implications for Changes in Sediment Delivery Processes in Some Tributaries of the Upper Yellow River in China. *ISPRS Int. J. Geo-Inf.* **2022**, *11*, 288. [[CrossRef](#)]
19. Valentin, C.; Poesen, J.; Li, Y. Gully erosion: Impacts, factors and control. *Catena* **2005**, *63*, 132–153. [[CrossRef](#)]
20. Prosdociimi, M.; Cerdà, A.; Tarolli, P. Soil water erosion on Mediterranean vineyards: A review. *Catena* **2016**, *141*, 1–21. [[CrossRef](#)]
21. Das, V.; Roy, S.; Barman, K.; Debnath, K.; Chaudhuri, S.; Mazumder, B. Investigations on undercutting processes of cohesive river bank. *Eng. Geol.* **2019**, *252*, 110–124. [[CrossRef](#)]
22. Das, V.; Roy, S.; Barman, K.; Chaudhuri, S.; Debnath, K. Study of clay–sand network structures and its effect on river bank erosion: An experimental approach. *Environ. Earth Sci.* **2019**, *78*, 591. [[CrossRef](#)]
23. Julian, J.; Torres, R. Hydraulic erosion of cohesive riverbanks. *Geomorphology* **2006**, *76*, 193–206. [[CrossRef](#)]
24. Yu, M.; Wei, H.; Wu, S. Experimental study on the bank erosion and interaction with near-bank bed evolution due to fluvial hydraulic force. *Int. J. Sediment Res.* **2015**, *30*, 81–89. [[CrossRef](#)]
25. Keawsawasvong, S.; Ukritchon, B. Undrained limiting pressure behind soil gaps in contiguous pile walls. *Comput. Geotech.* **2017**, *83*, 152–158. [[CrossRef](#)]
26. Keawsawasvong, S. Undrained stability of a spherical cavity in cohesive soils using finite element limit analysis. *J. Rock Mech. Geotech. Eng.* **2019**, *11*, 12. [[CrossRef](#)]
27. Qian, Z.; Li, A.; Merifield, R.; Lyamin, A. Slope Stability Charts for Two-Layered Purely Cohesive Soils Based on Finite-Element Limit Analysis Methods. *Int. J. Geomech.* **2015**, *15*, 06014022. [[CrossRef](#)]
28. Dapporto, S.; Rinaldi, M.; Casagli, N. Failure mechanisms and pore water pressure conditions: Analysis of a riverbank along the arno river (central Italy). *Eng. Geol.* **2001**, *61*, 221–242. [[CrossRef](#)]
29. Yodsomjai, W.; Keawsawasvong, S.; Thongchom, C.; Lawongkerd, J. Undrained stability of unsupported conical slopes in two-layered clays. *Innov. Infrastruct. Solut.* **2021**, *6*, 15. [[CrossRef](#)]
30. Li, A.; Lim, K.; Fatty, A. Stability evaluations of three-layered soil slopes based on extreme learning neural network. *J. Chin. Inst. Eng.* **2020**, *43*, 628–637. [[CrossRef](#)]
31. Gusman, M.; Nazki, A.; Putra, R. The modelling influence of water content to mechanical parameter of soil in analysis of slope stability. *J. Phys. Conf. Ser.* **2018**, *1008*, 012022. [[CrossRef](#)]
32. Hooke, J. An analysis of the processes of river bank erosion. *J. Hydrol.* **1979**, *42*, 39–62. [[CrossRef](#)]
33. Casagli, N.; Rinaldi, M.; Gargini, A.; Curini, A. Pore water pressure and streambank stability: Results from a monitoring site on the Sieve River, Italy. *Earth Surf. Process Landf.* **1999**, *24*, 1095–1114. [[CrossRef](#)]
34. Simon, A.; Curini, A.; Darby, S.; Langendoen, E. Bank and near-bank processes in an incised channel. *Geomorphology* **2000**, *35*, 193–217. [[CrossRef](#)]
35. Gu, T.; Zhang, M.; Wang, J.; Wang, C.; Xu, Y.; Wang, X. Slope edge irrigation and slope stability: Heifangtai platform, Gansu province, China. *Eng. Geol.* **2018**, *248*, 346–356. [[CrossRef](#)]
36. Aamir, M.; Ahmad, Z.; Pandey, M.; Khan, M.A.; Aldrees, A.; Mohamed, A. The Effect of Rough Rigid Apron on Scour Downstream of Sluice Gates. *Water* **2022**, *14*, 2223. [[CrossRef](#)]
37. Han, X.; Lin, P.; Parker, G. Influence of layout angles on river flow and local scour in grouped spur dikes field. *J. Hydrol.* **2022**, *614*, 128502. [[CrossRef](#)]
38. Pandey, M.; Pu, J.; Pourshahbaz, H.; Khan, M.A. Reduction of scour around circular piers using collars. *J. Flood Risk Manag.* **2022**, *15*, e12812. [[CrossRef](#)]
39. Huang, R.; Ni, Y.; Cao, Z. Coupled modeling of rainfall-induced floods and sediment transport at the catchment scale. *Int. J. Sediment Res.* **2022**, *37*, 715–728. [[CrossRef](#)]
40. Yang, Y.; Zheng, J.; Zhang, H.; Chai, Y.; Zhu, Y.; Wang, C. Impact of the Three Gorges Dam on riverbed scour and siltation of the middle reaches of the Yangtze River. *Earth Surf. Process Landf.* **2022**, *47*, 1514–1531. [[CrossRef](#)]
41. Yan, Y.; Zhang, X.; Liu, J.; Li, J.; Ding, C.; Qi, Z.; Shen, Q.; Guo, M. The effectiveness of selected vegetation communities in regulating runoff and soil loss from regraded gully banks in the Mollisol region of Northeast China. *Land Degrad. Dev.* **2021**, *32*, 2116–2129. [[CrossRef](#)]
42. He, L.; Chen, D.; Termini, D.; Jia, Y.; Zhang, Y. Modeling Bedload Transport Trajectories along a Sine-Generated Channel. *Water Resour.* **2019**, *46*, 542–552. [[CrossRef](#)]
43. Dey, L.; Barbhuiya, A.; Biswas, P. Experimental study on bank erosion and protection using submerged vane placed at an optimum angle in a 180° laboratory channel bend. *Geomorphology* **2017**, *283*, 32–40. [[CrossRef](#)]
44. Wang, X.; Xia, X.; Zhang, X.; Gu, X.; Zhang, Q. Probabilistic Risk Assessment of Soil Slope Stability Subjected to Water Drawdown by Finite Element Limit Analysis. *Appl. Sci.* **2022**, *12*, 10282. [[CrossRef](#)]
45. Sloan, S. Geotechnical stability analysis. *Géotechnique* **2013**, *63*, 531–572. [[CrossRef](#)]

46. Rao, P.; Zhao, L.; Chen, Q.; Nimbalkar, S. Three-dimensional limit analysis of slopes reinforced with piles in soils exhibiting heterogeneity and anisotropy in cohesion. *Soil Dyn. Earthq. Eng.* **2019**, *121*, 194–199. [[CrossRef](#)]
47. Maghous, S.; Saada, Z.; Garnier, D.; Dutra, V. Upper bound kinematic approach to seismic bearing capacity of strip foundations resting near rock slopes. *Eur. J. Environ. Civ. Eng.* **2022**, *26*, 3996–4019. [[CrossRef](#)]
48. Huang, W.; Loveridge, F.; Satyanaga, A. Translational upper bound limit analysis of shallow landslides accounting for pore pressure effects. *Comput. Geotech.* **2022**, *148*, 104841. [[CrossRef](#)]
49. Vasquez, J.A.; Steffler, P.M.; Millar, R.G. Modeling Bed Changes in Meandering Rivers Using Triangular Finite Elements. *J. Hydraul. Eng.* **2008**, *134*, 1348. [[CrossRef](#)]
50. Karssenber, D.; Bridg, J. A three-dimensional numerical model of sediment transport, erosion and deposition within a network of channel belts, floodplain and hill slope: Extrinsic and intrinsic controls on floodplain dynamics and alluvial architecture. *Sedimentology* **2008**, *55*, 1717–1745. [[CrossRef](#)]
51. Samadi, A.; Amiri-Tokaldany, E.; Davoudi, M.H.; Darby, S.E. Experimental and numerical investigation of the stability of overhanging riverbanks. *Geomorphology* **2013**, *184*, 1–19. [[CrossRef](#)]
52. Nardi, L.; Rinaldi, M.; Solari, L. An experimental investigation on mass failures occurring in a riverbank composed of sandy gravel. *Geomorphology* **2012**, *163*, 56–69. [[CrossRef](#)]
53. Fox, G.A.; Felice, R.G. Bank undercutting and tension failure by groundwater seepage: Predicting failure mechanisms. *Earth Surf. Process Landf.* **2014**, *39*, 758–765. [[CrossRef](#)]
54. Zhao, K.; Gong, Z.; Zhang, K.; Wang, K.; Jin, C.; Zhou, Z.; Xu, F.; Coco, G. Laboratory experiments of bank collapse: The role of bank height and nearbank water depth. *J. Geophys. Res. Earth Surface* **2020**, *125*, e2019JF005281. [[CrossRef](#)]
55. Du, J.; Yu, M.; Cong, Y.; Lv, H.; Yuan, Z. Soil Organic Carbon Storage in Urban Green Space and Its Influencing Factors: A Case Study of the 0–20 cm Soil Layer in Guangzhou City. *Land* **2022**, *11*, 1484. [[CrossRef](#)]
56. Lü, D.; Yu, C.; Zhuo, Z.; Meng, S.; Liu, S. The distribution and ecological risks of antibiotics in surface water in key cities along the lower reaches of the Yellow River: A case study of Kaifeng City, China. *China Geol.* **2022**, *5*, 411–420. [[CrossRef](#)]
57. Zhao, H.; Cheng, Y.; Zheng, R. Impact of the Digital Economy on PM<sub>2.5</sub>: Experience from the Middle and Lower Reaches of the Yellow River Basin. *Int. J. Environ. Res. Public Health* **2022**, *19*, 17094. [[CrossRef](#)]
58. Wang, Y.; Tian, H.; Xia, H.; Ge, S. Remote sensing monitoring of river channel changes in the section from Huayuankou to Liuyuankou of the Yellow River. *People's Yellow River* **2020**, *42*, 61–63. (In Chinese)
59. Thorne, C. Field measurements of rates of bank erosion and bank material strength // Erosion and Sediment Transport Measurement (Proceedings of the International Symposium). *Wallingford IAHS Publ.* **1981**, *133*, 503–512.
60. Xia, J.; Wu, B.; Wang, Y.; Zhao, S. An analysis of soil composition and mechanical properties of riverbanks in a braided reach of the Lower Yellow River. *Sci. Bull.* **2008**, *53*, 2400–2409. [[CrossRef](#)]
61. Nanjing Institute of Hydraulic Science. *Standard for Geotechnical Testing Method*; China Planning Press: Beijing, China, 2019. (In Chinese)
62. Abbo, A.; Wilson, D.; Sloan, S.; Lyamin, A. Undrained stability of wide rectangular tunnels. *Comput. Geotech.* **2013**, *53*, 46–59. [[CrossRef](#)]
63. Sall, O.; Sarr, D.; Makhaly, B.; Cisse, N.; Aboubacry, L. Numerical Analysis of Shallow Foundations in a Soil Mass under Various Behavior Laws. *Am. J. Sci.* **2019**, *7*, 129–137.
64. Keawsawasvong, S.; Ukritchon, B. Finite element limit analysis of pullout capacity of planar caissons in clay. *Comput. Geotech.* **2016**, *75*, 12–17. [[CrossRef](#)]
65. Moayedi, H.; Tien Bui, D.; Gör, M.; Pradhan, B.; Jaafari, A. The Feasibility of Three Prediction Techniques of the Artificial Neural Network, Adaptive Neuro-Fuzzy Inference System, and Hybrid Particle Swarm Optimization for Assessing the Safety Factor of Cohesive Slopes. *ISPRS Int. J. Geo-Inf.* **2019**, *8*, 391. [[CrossRef](#)]
66. Tschuchnigg, F.; Schweiger, H.; Lyamin, A.; Raissakis, I. Comparison of Finite-Element Limit Analysis and Strength Reduction Techniques. *Geotechnique* **2015**, *65*, 249–257. [[CrossRef](#)]
67. China Academy of Building Research. *Design Specifications for Building Foundations*; China Building Industry Press: Beijing, China, 2011. (In Chinese)
68. Wang, J. *Experimental Study on the Evolution Law of Curved Convex Banks under the Action of Unsaturated Sand-Carrying Currents*; Wuhan University: Wuhan, China, 2019. (In Chinese)
69. Wang, Y.; Kuang, S.; Su, J. Critical caving erosion width for cantilever failures of river bank. *Int. J. Sediment Res.* **2016**, *31*, 220–225. [[CrossRef](#)]
70. Zhang, K.; Gong, Z.; Zhao, K.; Wang, K.; Pan, S.; Coco, G. Experimental and Numerical Modeling of Overhanging Riverbank Stability. *J. Geophys. Res.* **2021**, *126*, e2021JF006109. [[CrossRef](#)]

**Disclaimer/Publisher's Note:** The statements, opinions and data contained in all publications are solely those of the individual author(s) and contributor(s) and not of MDPI and/or the editor(s). MDPI and/or the editor(s) disclaim responsibility for any injury to people or property resulting from any ideas, methods, instructions or products referred to in the content.